AGU PUBLICATIONS

JGR

Journal of Geophysical Research: Space Physics

RESEARCH ARTICLE
10.1002/2016JA023565

Key Points:
- Ionosonde and satellite measurements of the Weddell Sea Anomaly (WSA) can be reproduced with the FLIP model
- The longitudinal variation of the WSA electron density is caused by variations in both the neutral densities and the neutral winds
- The magnetic field configuration is only a minor factor in the longitudinal variation of the electron density in the WSA

Correspondence to:
P. G. Richards,
prichar1@gmu.edu

Citation:
Richards, P. G., R. R. Meier, S.-P. Chen, D. P. Drob, and P. Dandenault (2017), Investigation of the causes of the longitudinal variation of the electron density in the Weddell Sea Anomaly, *J. Geophys. Res. Space Physics*, *122*, 6562–6583, doi:10.1002/2016JA023565.

Received 7 OCT 2016
Accepted 18 MAY 2017
Accepted article online 24 MAY 2017
Published online 5 JUN 2017

Investigation of the causes of the longitudinal variation of the electron density in the Weddell Sea Anomaly

P. G. Richards[1], R. R. Meier[1], Shih-Ping Chen[2], D. P. Drob[3], and P. Dandenault[1]

[1]Department of Physics and Astronomy, George Mason University, Fairfax, Virginia, USA, [2]Institute of Space Science, Taiwan Geospace Studies, National Central University of Taiwan, Jhongli, Taiwan, [3]Space Science Division, Naval Research Laboratory, Washington, District of Columbia, USA

Abstract This paper investigates and quantifies the causes of the Weddell Sea Anomaly (WSA), a region near the tip of South America extending from approximately 30° to 120°W geographic longitude and 50° to 75°S geographic latitude at solar minimum between 2007 and 2010. This region is unusual because the midnight peak electron density exceeds the midday peak electron density in summer. This study is far more quantitative than previous studies because, unlike other models, it assimilates selected data parameters to constrain a physical model in order to investigate other aspects of the data. It is shown that the commonly accepted explanation that the WSA is related to the magnetic field declination and inclination effects on the neutral wind does not explain the longitudinal variation of the electron density. Rather, longitudinal changes in the neutral winds and neutral densities are the most likely explanation for the WSA. These longitudinal wind and density changes are attributed to the varying latitudinal distance from the auroral zone energy input. No contributions from the plasmasphere or other sources are required. Furthermore, it is shown that a widely used empirical thermosphere density model overestimates the longitudinal changes in the WSA region.

Plain Language Summary This paper investigates and quantifies the causes of the Weddell Sea Anomaly (WSA), a region near the tip of South America extending from approximately 30° to 120°W geographic longitude and 50° to 75°S geographic latitude at solar minimum between 2007 and 2010. This region is unusual because the midnight peak electron density exceeds the midday peak electron density in summer. This study is far more quantitative than previous studies because, unlike other models, it assimilates selected data parameters to constrain a physical model in order to investigate other aspects of the data. It is shown that the commonly accepted explanation that the WSA is related to the magnetic field declination and inclination effects on the neutral wind does not explain the longitudinal variation of the electron density. Rather, longitudinal changes in the neutral winds and neutral densities are the most likely explanation for the WSA. These longitudinal wind and density changes are attributed to the varying latitudinal distance from the auroral zone energy input. No contributions from the plasmasphere or other sources are required. Furthermore, it is shown that a widely used empirical thermosphere density model overestimates the longitudinal changes in the WSA region.

1. Introduction

This research examines and quantifies the causes of the anomalous diurnal behavior of the ionospheric electron density in the southeast Pacific Ocean where the midnight peak electron densities exceed the midday values in summer, which is the reverse of normal ionosphere behavior. The Weddell Sea Anomaly (WSA) was initially identified in ionosonde data in the 1950s by *Bellchambers and Piggott* [1958] who noted that the midnight to noon f_oF_2 ratio was greater than unity in summer in the Weddell Sea at Halley Bay (76°S, 27°W). Thus, this anomaly became known as the Weddell Sea Anomaly (WSA). Later, it was found that the heart of anomaly is actually located in the southeast Pacific Ocean rather than the South Atlantic Ocean. This study uses ionosonde and satellite data together with the field line interhemispheric plasma (FLIP) physical model to explore the causes of the anomaly.

In summer, there are large regions of the midlatitude ionosphere in both hemispheres where the maximum electron density (N_mF_2) occurs at or just after sunset rather than at noon, which is contrary to expectation. What distinguishes the WSA from the other regions that have nighttime maxima is that the maximum density occurs near midnight. Figure 1 shows the global midnight to midday N_mF_2 ratio from the FORMOSAT-3/

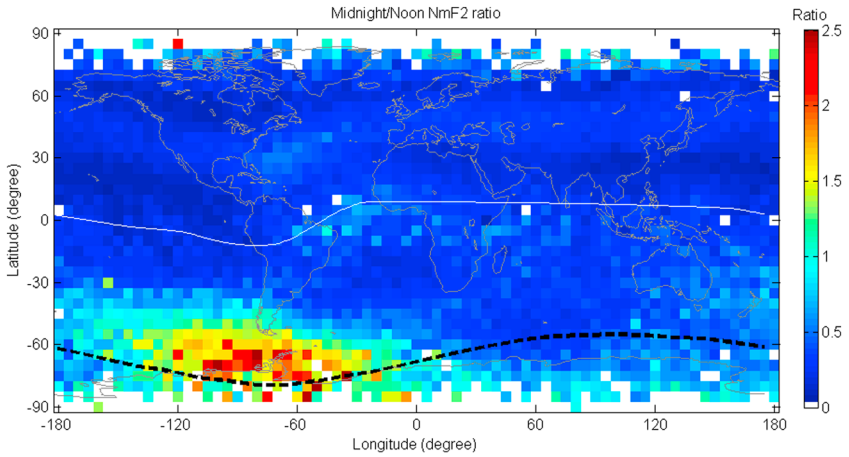

Figure 1. Map showing the midnight to midday N_mF_2 ratio of the combined January and December COSMIC N_mF_2 data from all the years 2007 to 2010. The black dashed line in the Southern Hemisphere is for −66° magnetic latitude (L = 6).

Constellation Observing System for Meteorology, Ionosphere, and Climate (COSMIC) satellite constellation radio occultation data. COSMIC is a joint Taiwan-U.S. mission, consisting of six microsatellites (see *Burns et al.* [2008] and *Lin et al.* [2009] for a description of COSMIC). All data from December and January and the years 2007 to 2013 were combined to create Figure 1. The binning was ±1 h around noon and midnight. The WSA clearly stands out in the Southern Hemisphere between about 30°W and 150°W longitude. The dashed black line in Figure 1 is for 66°S magnetic latitude (L = 6).

Remote sensing and in situ observations demonstrated that the WSA extends over a large region in the southern central Pacific region with a maximum to the west of the tip of South America [*Horvath and Essex*. 2003; *Lin et al*., 2009, 2010; *He et al*., 2009; *Jee et al*., 2009; *Liu et al*., 2011]. *Lin et al.* [2010] used COSMIC data for 2007 to show that there is a prominent electron density enhancement at 2200 LT from November to February for longitudes near the tip of South America, but it is most intense in December and January. The COSMIC data show a similar but much less dramatic anomaly near the Bering Sea in the Northern Hemisphere in June. The unusual *F* layer nighttime electron density enhancements were further characterized by the radio occultation observations from the COSMIC constellation by *Burns et al.* [2008]. *Lin et al*. [2009] illustrated the three-dimensional electron density structure of the WSA with COSMIC data. The WSA and other nighttime anomalies have also been observed in the 1356 Å O^+ + e recombination emission by the Thermosphere Ionosphere Mesosphere Energetics and Dynamics (TIMED)-GUVI (Global Ultraviolet Imager) instrument [*Hsu et al*., 2011].

Horvath [2006], *He et al.* [2009], *Chen et al.* [2016], and others have attributed the WSA to the variation in the magnetic field declination and inclination acting in conjunction with the neutral wind. Such an explanation implies that there is little or no variation in the geographical wind components with longitude. Otherwise, longitudinal variation in the winds could negate the effects of the magnetic field structure. Northward winds, which are positive and blow toward the equator, raise h_mF_2, while poleward winds lower h_mF_2. The inclination changes the component of the winds that drives the ions along the magnetic field. A change in declination modifies the wind in the magnetic meridian by altering the relative contributions of geographic meridional and zonal winds. The arrows in Figure 2 show the magnetic declination at 65°S geographic latitude. The region where the midnight to noon density ratio exceeds unity lies between 00°W and 150°W. The ellipse in Figure 2 shows the approximate region where the N_mF_2 ratio is greater than 2. Table 1 lists the magnetic declination and other key parameters. The magnetic declination explanation seems unlikely to completely explain the WSA because, as shown by the arrows in Figure 2, the change in magnetic declination across the edges of the WSA (see the relatively sharp gradient in Figure 1) are small and the declination has opposite signs on the east and west edges. Another difficulty with this explanation is that a change in declination can simultaneously increase one wind component along the field line and decrease the other component depending on the direction of the geographic meridional and zonal components.

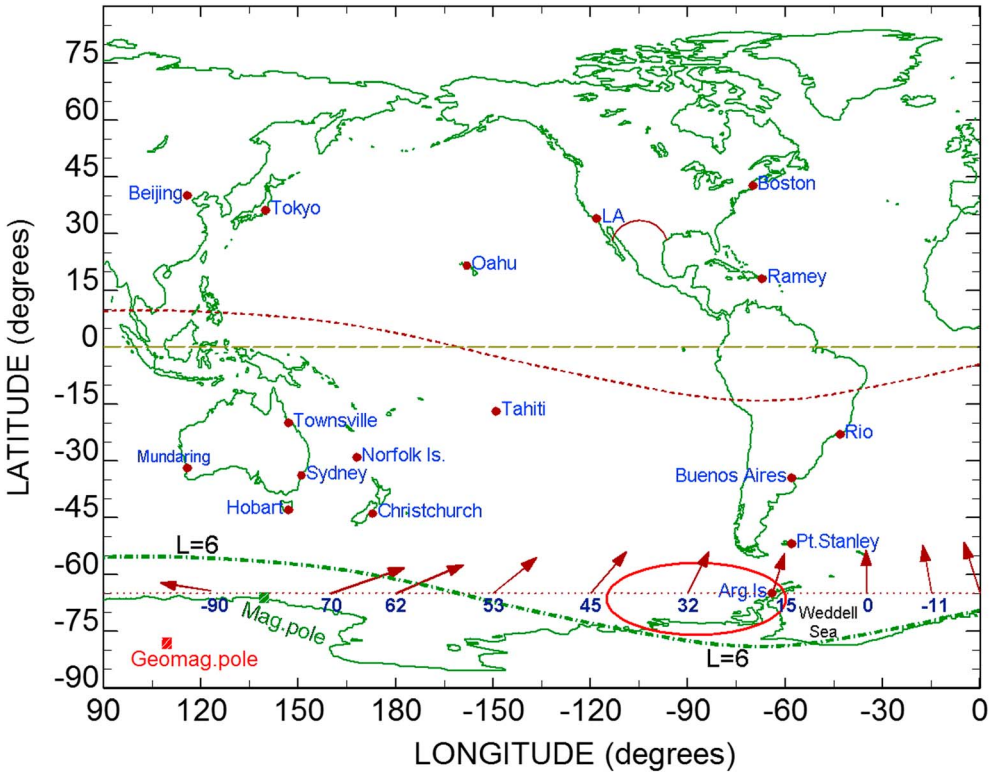

Figure 2. Map showing the magnetic declination at 65°S latitude. The ellipse shows the approximate location of the main Weddell Sea Anomaly region where the midnight N_mF_2 exceeds the midday N_mF_2 by a factor of 2. The arrows show the declination from geographic meridian pictorially. The numbers underneath the arrows give the magnitude of the declination. Dip angle and other magnetic parameters are displayed in Table 1. The geographic and geomagnetic equators are also shown. The dash-dotted line shows the approximate L = 6 (66°S magnetic latitude) contour. Also shown are the magnetic (65°S, 138°E) and geomagnetic (80°S, 108°E) poles. The magnetic pole is where the field lines are vertical, and the geomagnetic pole is the point where the axis of a centered dipole intersects the Earth's surface.

High-magnetic latitudes are not modeled in this paper because the highly variable particle precipitation, ion convection, and ion-neutral drag make it very difficult for any model to produce reliable results. For example, the 2007–2010 incoherent scatter radar data from Poker Flat (65°N, 147°W, $L \approx 6$) reveal order of magnitude electron density depletions near midnight in summer even during low magnetic activity [*Richards et al.*, 2014]. These depletions, which are caused by strong ion convection, counteract any tendency to form midnight density enhancements at high magnetic latitudes. Consequently, the current research concentrates on the region between 00°W and 150°W longitudes at 65°S to avoid the auroral zone, which is indicated approximately by the L = 6 (magnetic latitude = 66°S) line in Figures 1 and 2. The 65°S geographic latitude was chosen because it runs through the center of the WSA and because there are three solar cycles worth of ionosonde data available from the Argentine Islands.

Table 1. Magnetic Field Parameters at Geographic Latitude 65°S as a Function of Geographic West Longitude (Glong)[a]

Glong	D	I	Mlat	L	Cos$D$	Sin$D$	sin$I$ × Cos$I$
0	−20	61	−58	3.8	0.94	−0.34	−0.42
−35	−2	59	−56	3.3	1.00	−0.03	0.44
−65	16	59	−50	2.6	0.96	0.28	0.44
−95	33	63	−51	2.7	0.84	0.54	0.40
−120	44	68	−56	3.3	0.72	0.69	0.35
−150	52	75	−62	4.7	0.62	0.79	0.25

[a] D = declination, I = inclination, Mlat = magnetic latitude, and L = L value.

There have been several theoretical studies of the WSA with ionosphere-thermosphere general circulation models that have yielded inconclusive results [*Fuller-Rowell et al.*, 1996; *Burns et al.*, 2011]. While global general circulation models (GCMs) can provide valuable insights into the physics of the ionosphere-

thermosphere system, quantitative evaluation of certain phenomena can be impaired by nonlinear interactions between the neutral winds, neutral composition, and ionosphere, and by the inability to accurately specify of the external drivers of the system. Indeed, *Burns et al*. [2008, 2011] concluded that there is no unambiguous explanation of the WSA.

An alternative approach by *Chen et al*. [2011] used the first-principles SAMI2 (Sami2 is Another Model of the Ionosphere) model of *Huba et al*. [2000] to gain geophysical insight into some of the characteristics of the anomaly. The SAMI2 model solves a similar set of equations to the FLIP model with observationally based empirical models used to specify the neutral winds and composition. The SAMI2 model does produce a nighttime enhancement in the vicinity of the Weddell Sea, but there were some differences from the observations. For example, the anomaly was weak at the Argentine Islands where numerous observations show it to be very strong. *Chen et al*. [2011] identified the equatorward neutral wind as the major cause of the WSA together with a downward flux of plasma from the plasmasphere. *Ren et al*. [2012] used a similar approach and also concluded that winds are responsible for the WSA.

Karpachev et al. [2010, 2011] studied the WSA using Intercosmos and CHAMP satellite data and modeling and concluded that it is mainly caused by the neutral wind both from longitudinal variations in the velocity and magnetic field configuration but that further study would be needed with improved neutral winds. They discounted neutral atmosphere effects and nighttime plasma flows from the plasmasphere. *Klimenko et al*. [2015] used topside sounder and ionosonde data together with a first-principles model and concluded that the WSA is caused by neutral winds and composition. They also suggest that horizontal transport from electromagnetic drifts is needed to explain the high nighttime densities.

Chang et al. [2015] examined COSMIC observations of total electron content (TEC) and electron densities to identify the tidal and stationary planetary wave signatures in the ionosphere that contribute to the generation of the WSA. They found that the amplitudes and phases of the diurnal and semidiurnal westward migrating tidal signatures (e.g., DW1 and DW2) are enhanced in the southern middle to high magnetic latitudes during the southern summer, with peak amplitudes around 300 km altitude. These interannual recurring features indicate that the tides superimpose near the midnight hours in the Antarctic Peninsula region to create the WSA the peak in electron density.

In this work, we present quantitative evidence for the hypothesis that longitudinal variations in both the neutral densities and winds play key roles in the WSA behavior. As shown in Figure 2, for a constant geographic latitude, the WSA region is located farthest from the auroral zone in the Southern Hemisphere, and therefore, the neutral densities and winds are least likely to be directly influenced by auroral energy input. The correlation of densities and winds with distance from the auroral zone can explain the anomalous ionospheric behavior as well as account for the correlation with declination and inclination reported by *Horvath* [2006].

This study is facilitated by the availability of comprehensive databases, including ionosonde and COSMIC data sets, neutral composition and temperature from TIMED-GUVI (Global Ultraviolet Imager) [*Christensen et al*., 2003], and solar EUV irradiance measurements from the Solar EUV Experiment instrument on TIMED [*Woods et al*., 2008].

The FLIP model is ideally suited to investigate the WSA because it combines an accurate representation of the Earth's magnetic field with comprehensive photochemistry. An important advantage of the current study over previous studies is that FLIP model can assimilate the observed height of the peak electron density (h_mF_2). This capability is essential for reducing the large uncertainties in the electron density that can arise from uncertainties in the neutral wind. Indeed, it is not possible to accurately model the electron density with a model that does not reproduce the measured h_mF_2 to within a few kilometers on average.

Our main finding is that the longitudinal variation of the anomaly is primarily caused by longitudinal variations in the neutral density and wind. We demonstrate that the magnetic field orientation has at most a small effect on the longitudinal variation of the electron density in the WSA. Further, plasma fluxes from the plasmasphere cannot account for the WSA because they are upward, not downward as proposed in earlier work.

2. Data

2.1. Ionosonde h_mF_2 and N_mF_2

A large amount of ionosonde data spanning the years 1961 to 1990 is available on CD-ROM from the National Geophysical Data Center (NGDC). Data from 1990 to the present are available from the NGDC-Space Physics Interactive Data Resource web site. Two different formulae have been commonly used by the ionospheric community to retrieve h_mF_2 from ionosonde measurements of the critical frequencies of the F_2 layer, the E layer (f_oE), and the maximum usable frequency (($M3000)F_2$). Many studies have used the formula presented by *Dudeney* [1983], while the International Reference Ionosphere [*Bilitza*, 2015] model uses the formula due to *Bilitza et al*. [1979], which we use for the calculations in this paper. It yields median h_mF_2 values that are ~2 km larger than the *Dudeney* [1983] formula for the summer solar minimum conditions under investigation here. Such a small difference does not affect the conclusions in this article.

This study also uses 2007 to 2010 from the Australian ionospheric prediction service (http://www.ips.gov.au/). These stations are Canberra (35°S, 149°E, L = 1.9), Hobart (43°S, 147°E, L = 2.57), Macquarie Island (55°S, 159°E, L = 4.2), Mundaring, (32°S, 116°E, L = 1.9), Norfolk Island (29°S, 168°E, L = 1.5), Townsville (20°S, 147°E, L = 1.3), and Christchurch (44°S, 173°E). These data are carefully hand scaled, which have been shown to be more accurate than automatic scaling.

2.2. COSMIC h_mF_2 and N_mF_2

COSMIC is a joint Taiwan-U.S. mission, consisting of six microsatellites that were launched in April 2006 into a 500 km altitude orbit and are now in near circular orbit at altitudes around 800 km. The raw observations are processed in both near real-time and postprocess modes and stored at the COSMIC Data Analysis and Archive Center (CDAAC). Electron density profiles are retrieved from the COSMIC Ionospheric Radio Occultation (IRO) measurements via an Abel transform of slant TEC measurements. To determine the primary ionosphere parameters, all COSMIC Ne profiles within the altitude range of 170–600 km are fitted one-by-one with a least squares procedure using a Chapman function [*Chapman*. 1931; *Rishbeth and Garriott*, 1969]. This fitting technique has been described by *Liu et al*. [2011, and references therein] in analyzing Ne profiles from the incoherent scatter radar observations and IRO measurements. According to the error analysis by *Yue et al*. [2010], the standard deviations of the differences between the retrieved and true values are ~16% N_mF_2 and ~2% for h_mF_2. This means that the largest errors for January (~7 km) occur near midnight when the layer is near 300 km. In order to obtain sufficient coverage, we selected COSMIC data for 21 day intervals centered on January for the years 2007–2010. The data have been summed into half hour bins.

2.3. TIMED-GUVI Neutral Densities and Temperature

Meier et al. [2015] and by *Emmert et al*. [2006, 2014] have described the techniques for obtaining the altitude profiles of the densities and temperatures from the Global Ultraviolet Imager (GUVI) instrument on board the Thermosphere Ionosphere Mesosphere Energetics and Dynamics (TIMED) satellite.

3. FLIP Model

The field line interhemispheric plasma (FLIP) model has been developed over a period of more than 25 years as a tool specifically designed to improve our understanding of the physics and chemistry of the ionosphere [*Richards et al*., 1998, 2000, 2010; *Richards and Wilkinson*, 1998; *Richards*, 2001, 2002, 2004; *Torr et al*., 1990; *Kotov et al*., 2015].

The most important requirement for accurately modeling N_mF_2 and the whole electron density altitude profile is to reproduce the observed h_mF_2, because the recombination rate depends on altitude through the molecular concentrations. For given geophysical conditions, h_mF_2 is, in turn, primarily dependent on the neutral winds at midlatitudes [*Richards*, 1991]. The FLIP model has the capability to ingest any measured or model winds from a file or use empirical models such as the horizontal wind model-14 (HWM14) [*Drob et al*., 2015]. If h_mF_2 measurements are available, the preferred option is for the model to automatically adjust neutral winds to accurately reproduce the observed h_mF_2 as it steps in time [*Richards*, 1991]. The resulting winds are termed equivalent or effective winds because some changes in h_mF_2 may also be caused by zonal electric fields [*Rishbeth*, 1972]. The inclusion of electric fields is a bonus for ionospheric electron density modeling as both winds and electric fields are needed to produce accurate electron densities. Under magnetically quiet

conditions, electric field effects appear to be small at magnetic midlatitudes as several studies have shown good agreement between equivalent winds and optical wind measurements [e.g., *Dyson et al*., 1997; *Richards et al*., 2009].

There are several sources of uncertainties in the calculated magnetic meridional equivalent winds. These include uncertainties in (1) h_mF_2, (2) atomic oxygen density, (3) the O^{+}-O collision frequency, and (4) the possible presence of electric fields. Errors in the measured h_mF_2 are only important if they are systematic because random h_mF_2 errors are effectively averaged out by the FLIP model procedure. For January 2007–2010 the COSMIC h_mF_2 is systematically 10–15 km lower than ionosonde h_mF_2 at Christchurch. FLIP model calculations indicate that a 15 km increase in h_mF_2 would increase the midnight equatorward wind speed by about 30 m/s. Measurements and the NRLMSISE-00 thermosphere model [*Picone et al*., 2002] indicate that the atomic oxygen density is very reliable near 300 km even during magnetic disturbances (see discussion by *Richards et al*. [2010]).

With respect to the collision frequency, early comparisons of optical wind measurements with those inferred from incoherent scatter radars by *Burnside et al*. [1987] produced a value of 1.7 as a multiplicative factor for the collision frequency of *Schunk and Walker* [1973]. This led to the adoption of the so-called Burnside factor of 1.7 by the aeronomy community [*Salah*, 1993]. Recent theoretical calculations and independent evaluations of the optical and radar data yield estimates of the "Burnside" factor ranging from 0.85 to 1.4 [e.g., *Nicolls et al*., 2006; *Jee et al*., 2005; *Anderson et al*., 2012; *Wu et al*., 2012]. The incoherent scatter technique also uses the collision frequency to derive neutral winds from the ion velocity. The incoherent scatter radar community has adopted a Burnside factor of 1.3 [*Nicolls et al*., 2006], and that is the factor that is used for the calculations in this paper. The magnitude of the collision frequency has little effect during the day when the ionosphere is primarily driven by photoionization. However, FLIP model calculations indicate that a 30% decrease in the collision frequency increases the equivalent winds at midnight by ~25 m/s. On the other hand, when using the HWM winds, a 30% decrease in the collision frequency decreases the model h_mF_2 by ~15 km at night. It should be emphasized that the FLIP model N_mF_2 is insensitive to the collision frequency when the model assimilates h_mF_2.

Both electric fields and winds are necessary for modeling the ionosphere electron density. And using h_mF_2 as the wind proxy takes care of both. If the electric fields are random, they will not have a significant effect on the equivalent winds. However, it is necessary to be aware of the possibility of systematic electric fields effects when comparing equivalent winds with empirical models or to measurements by optical or radar methods.

Satellite data are not optimal for ingesting into the model because the measurements are not contiguous in time and space. Consequently, we use medians of the COSMIC data collected over 1–18 January in 2007, 2008, 2009, and 2010. To compare the model N_mF_2 with the median COSMIC N_mF_2, median model values matching the observational conditions were determined from calculations made for 1–18 January for each of the same years, using the median h_mF_2 as the wind proxy for each year. Median model N_mF_2 values were determined for each UT hour that could be compared with the COSMIC measured median N_mF_2. This approach is required in order to accommodate solar and magnetic activity variations from 2007 and 2010.

To check the validity of using the COSMIC median h_mF_2 values, two separate calculations were performed using the Argentine Islands ionosonde data from the six solar minimum years between 1975 and 1987. First, the hourly median model N_mF_2 was calculated from the 6×15 values created by running the model using the observed hourly h_mF_2 values as the wind proxy for 1–15 January for each of the 6 years. Then the calculations were repeated using the measured median h_mF_2 instead of the hourly values. It was found that the median N_mF_2 values calculated using the median h_mF_2 values were not significantly different from the medians obtained using the hourly h_mF_2 ionosonde h_mF_2 data, thereby validating our approach.

For the neutral atmosphere, the FLIP model uses the NRLMSISE-00 model which is known to reproduce average satellite drag and mass spectrometer data to within ~15%. However, during ionospheric storms there may be large differences between measurement and model and NRLMSISE-00 for the atomic to molecular neutral density ratio, to which the electron density bears a direct dependence in photochemical equilibrium [*Richards et al*., 2010]. *Richards et al*. [1998, 2009, 2010] developed a new algorithm that estimates changes to the NRLMSISE-00 atomic to molecular density ratio that are needed to explain differences between the

measured and modeled N_mF_2. For convenience, this paper refers to the O to N_2 density ratio rather than atomic to molecular (N_2 and O_2) density ratio. However, the recombination reaction with O_2 is also an important loss of O^+. The FLIP model calculations indicate that the N_2 loss rate at h_mF_2 is a factor of 2 greater than the loss rate to O_2 at noon and a factor of 3 greater at midnight in the center of the WSA. Because O_2 and N_2 have similar masses, their variations tend to track one another.

4. Results: Observing and Modeling the WSA

The following calculations take advantage of the FLIP model's ability to assimilate selected data as input parameters. In particular, the ability to incorporate the observed h_mF_2 overcomes the problem that other models have with accurately specifying the neutral wind. In this results section we establish the capability of the FLIP model to reproduce the ionosonde observed N_mF_2 at the Argentine Islands in the heart of the WSA; present the longitudinal variation of the COSMIC satellite h_mF_2 and N_mF_2 data from the eastern to the western perimeters of the WSA; derive equivalent winds from the observed h_mF_2 and use them in a new way to determine the longitudinal variation of the geographic meridional and zonal wind components; use longitudinally invariant geographic neutral winds to isolate the effects of magnetic declination and inclination on h_mF_2; and explore the role of the longitudinal variation of neutral densities using GUVI observations and model calculations.

The calculations show that longitudinal variation of both densities and winds are the most important factors for explaining the observed N_mF_2 longitudinal behavior across the WSA. The calculations also show that plasmaspheric fluxes do not contribute to the high nighttime electron densities.

4.1. Argentine Islands Behavior

Three decades of ionosonde data show that the anomaly is particularly large at the Argentine Islands (65°S, 64°W). It is present at all levels of solar activity during the summer period from the beginning of November until the end of February and is absent only during major magnetic disturbances.

Figure 3 shows the model (lines) and data (solid red circles) for 22–26 January 1975 when the magnetic and solar activity levels were low to moderate. The measured N_mF_2 is a factor of 2 larger at midnight than at noon. All of the solid blue lines in Figure 3 are from the FLIP model calculation using the observed h_mF_2 as a wind proxy.

There are 7567 data points from hourly ionosonde solar minimum data during December and January in the years 1975, 1976, 1977, 1985, 1986, and 1986. The average time of occurrence for the maximum nighttime N_mF_2 is ~00 LT, the average N_mF_2 is $(6.7 \pm 2.0) \times 10^5$ cm^{-3}, and the average h_mF_2 is 338 ± 22 km. The average minimum N_mF_2 is $(3.2 \pm 0.8) \times 10^5$ cm^{-3}, which occurs at ~14 LT when the average h_mF_2 is 246 ± 26 km. The FLIP model reproduces the observed Argentine Islands behavior very well not only at these solar minimum conditions but also at all other levels of solar activity, using the standard NRLMSISE-00 model densities.

The long dashed line in Figure 3a is the O^+ density at h_mF_2 that is determined from photochemical equilibrium (production rate = loss rate, without diffusion). It maximizes near midnight when the O/N_2 number density ratio at h_mF_2 maximizes (Figure 3e). Note that the photoionization rate is still significant at midnight because the solar zenith angle never exceeds 95° at 65°S during this period. At 300 km, the slant optical depth (τ) to the Sun is ~0.16 and the solar flux attenuation factor for the major photoionization wavelengths ($e^{-\tau}$) is ~0.85 at midnight. Variation in the attenuation of the solar flux could be a small factor (~10%) contributing to the longitudinal variation of N_mF_2 if there is a significant longitudinal variation in h_mF_2 or in the neutral densities when the solar zenith angle is near 90°. Both of these factors determine the column density that the solar radiation must traverse to reach h_mF_2. When h_mF_2 is slightly lower, there is more absorption but the photoionization rate can be comparable because the O density is higher.

The FLIP model produces a lower density than pure photochemical equilibrium at night because excess production of O^+ near and above h_mF_2 is removed primarily by diffusion to lower altitudes where the loss rates are larger; although the equatorward wind impedes the downward diffusion of ions. Downward diffusion is also the reason that the model N_mF_2 is larger than the chemical equilibrium value during the daytime because excess production from above h_mF_2 is transported down with the help of poleward winds.

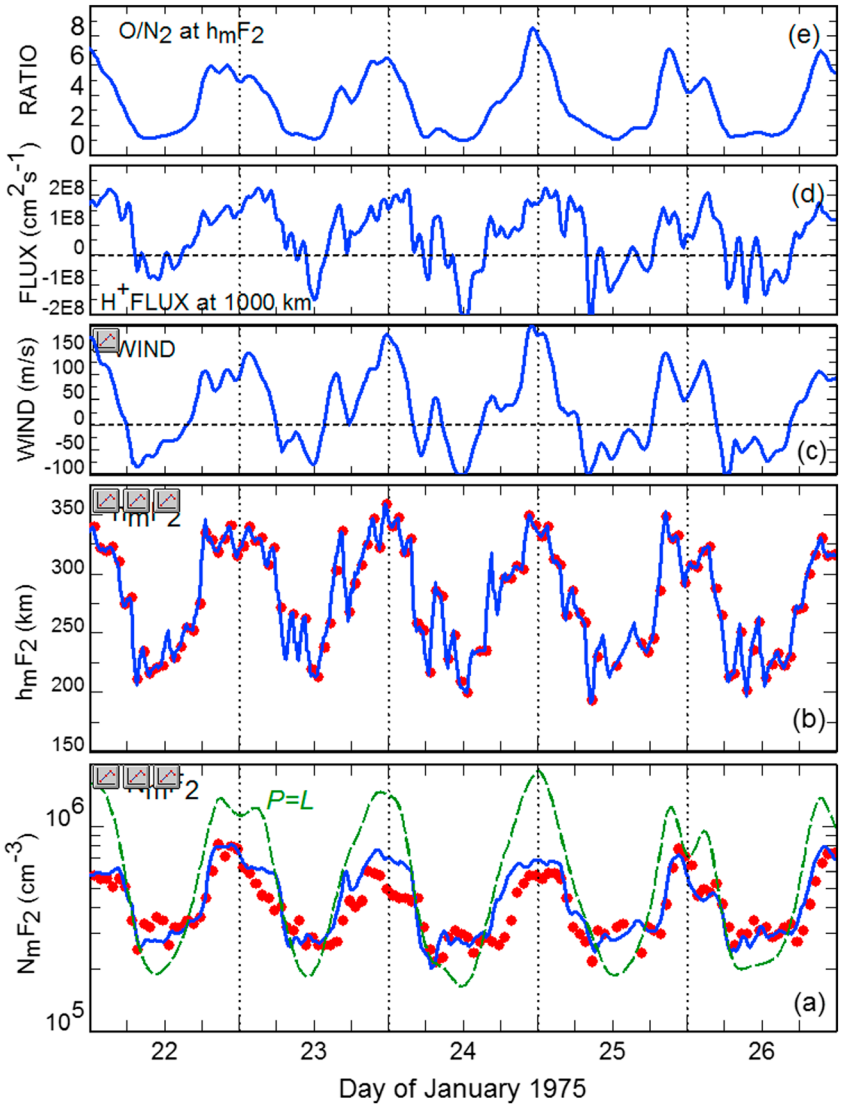

Figure 3. Measured (red dots) and modeled (lines) N_mF_2 and h_mF_2 at Argentine Island (65°S, 64°W) for 22–26 January 1975. The solid blue lines show the FLIP model (a) N_mF_2, (b) h_mF_2, (c) magnetic meridional wind, (d) plasmaspheric H^+ flux, and (e) O/N_2 ratio at 1000 km. The long dashed green N_mF_2 line ($P = L$) is the chemical equilibrium O^+ density at h_mF_2. The vertical grid lines are at midnight LT.

The magnitude of the chemical equilibrium density in Figure 3a shows that local production at h_mF_2, by itself, is more than adequate to produce the observed nighttime density. Several researchers have argued that the downward fluxes of ionization from the plasmasphere contribute to the high electron densities at night [e.g., *Chen et al.*, 2011]. However, Figure 3d shows that the FLIP model topside H^+ flux at 1000 km is actually upward (positive) at night, leading to a small net loss of O^+ from the ionosphere to the plasmasphere through charge exchange. This is consistent with the finding of *Karpachev et al.* [2011]. The nighttime upward flux is to be expected as plasma will naturally flow from the hot sunlit summer hemisphere toward the relatively cold winter hemisphere, which is dark for more than 12 h.

The solid blue line in Figure 3b shows how closely the FLIP model follows the measured h_mF_2. The model-data differences are typically less than 5 km. Any missing h_mF_2 values are replaced by a running mean for the same UT on previous days. Only actual data points (not means) are plotted in the figures. Figure 3c shows the horizontal wind in the magnetic meridian. Northward (positive) winds blow toward the equator and raise h_mF_2, while poleward winds lower h_mF_2.

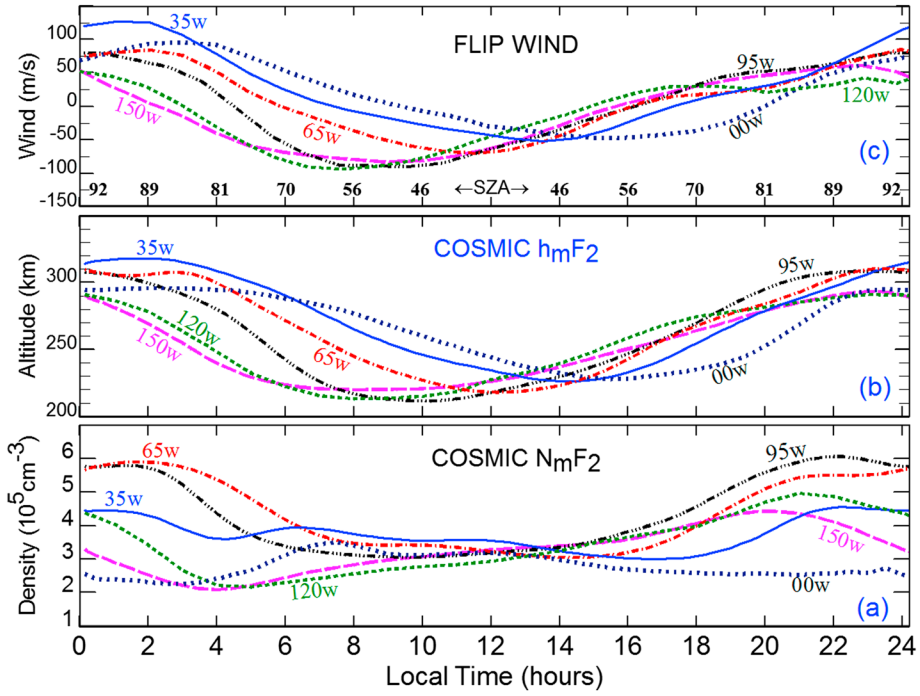

Figure 4. The COSMIC measurements of (a) N_mF_2 and (b) h_mF_2 across the WSA at 65°S latitude and 0°W, 35°W, 64°W, 95°W, 120°W, and 150°W longitudes during 1–18 January of 2007 to 2010. The COSMIC data are binned on the half hour. (c) The equivalent winds determined from the COSMIC h_mF_2 in Figure 4b. The solar zenith angel (SZA) is shown in Figure 4c.

Figure 3 demonstrates that the FLIP model can reproduce the observed N_mF_2 behavior in the heart of the WSA, given the appropriate h_mF_2 (or winds plus electric fields). It is therefore possible to address quantitatively the fundamental question, "What are the causes of the observed longitudinal variation of the electron density across the WSA region?"

4.2. COSMIC h_mF_2 and N_mF_2 Across the WSA

This study is limited to 65°S geographic latitude and the longitude region between 00°W and 150°W that is least affected by the highly variable high-latitude processes that cannot be accurately characterized in any model. At 65°S, 150°W corresponds to 62°S magnetic latitude ($L = 4.7$). This would put it just outside the auroral oval most of the time for the solar minimum conditions considered here.

Since the WSA is defined in terms of the ratio of the midnight to noon N_mF_2, the time period between noon and midnight is of primary interest in this study. Although there is no anomaly in the COSMIC data at 00 W and 150 W under this definition, they are included in this study to illuminate the factors that limit the area of the WSA. It is important to note that the electron density at midnight depends to some extent on the history of the wind and neutral density variations in the preceding hours.

Figures 4a and 4b show the local time variation of the COSMIC N_mF_2 and h_mF_2 data at seven longitudes spanning the WSA region at 65°S latitude during 1–18 January of 2007–2010. The COSMIC data are binned on the half hour, local time. Clearly, the anomalous electron density ratio across the WSA is a purely nighttime phenomenon because there are negligible longitudinal changes in the noon N_mF_2. Except for 00°W, the longitudinal differences in h_mF_2 are small ($<$ 20 km) between noon and midnight.

4.3. COSMIC h_mF_2 and Neutral Winds

Figure 4c shows the equivalent neutral winds in the magnetic meridian that were determined from the COSMIC h_mF_2 in Figure 4b using the algorithm of *Richards* [1991]. As expected, the neutral winds reflect the diurnal variation of h_mF_2. And, just like h_mF_2, there is little longitudinal difference in the winds between noon and midnight, except for 00°W. This contrasts with the large longitudinal differences in h_mF_2 between

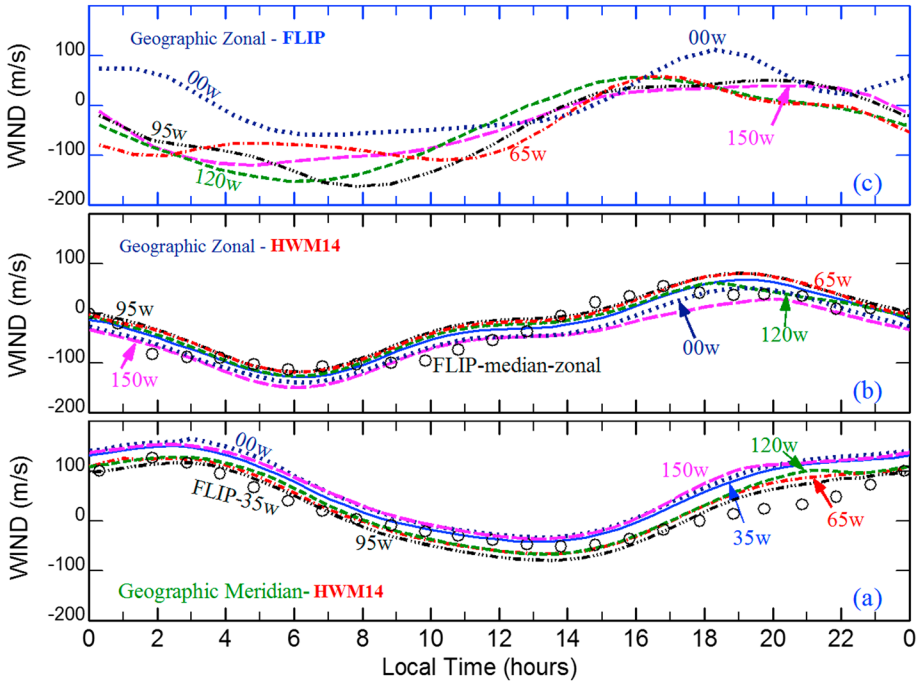

Figure 5. Geographic meridional and zonal neutral winds at 65°S latitude and 0°W, 35°W, 64°W, 95°W, 120°W, and 150°W longitudes. (a) HWM14 meridional winds, (b) HWM14 zonal winds, and (c) zonal winds calculated from the equivalent winds in Figure 4c assuming the 35°W FLIP model equivalent wind is purely in the geographic meridian. The open circles show on Figure 5a show the FLIP model wind at 35°W. The open circles in Figure 5b show the median FLIP model zonal wind from the winds in Figure 5c. For each longitude, these winds are medians at each local time over 1–18 January 2007–2010.

midnight and noon, which can be attributed to the effect of magnetic declination when the zonal wind speeds are large and negative, as will be demonstrated next.

The longitudinal similarities and differences are revealed in more detail through their geographic and magnetic meridian wind components plotted in Figures 5 and 6. Figures 5a and 5b show the longitudinal variation in the HWM14 winds in the geographic meridian and zonal directions, respectively, for the same longitudes as in Figure 4. These wind components do not have the phase shifts between midnight and noon that are evident in the FLIP model magnetic meridional winds shown in Figure 4c. Nor do they have much longitudinal variation. Also, in the center of the anomaly at 65°W and 95°W the HWM14 meridional winds overlap and there is little difference between the 00°W, 35°W, and 150°W meridional winds on the two edges of the anomaly. The diurnal variation of the FLIP model equivalent wind at 35°W is also shown in Figure 5a (open circles) because the small declination (~2°W) means that it is almost entirely in the geographic meridian.

Implicit in the hypothesis by previous workers that the WSA arises from the varying magnetic field configuration is the assumption that there is little or no variation in the geographic zonal and meridional winds. If we assume that the diurnal variation of the meridional wind is the same at all longitudes and equal to that at 35°W (where the magnetic and geographic meridians are the same), we can estimate the geographic zonal component of the winds at the other longitudes from the FLIP model magnetic meridional winds from

$$W_{zon=}\left(W_{mer}\cos D - W_{eq}\right)/\quad \sin D, \tag{1}$$

where W_{zon} is the geographic zonal wind component to be evaluated, W_{mer} is the FLIP model geographic meridional component for 35°W, W_{eq} is the FLIP model equivalent wind in the magnetic meridian from Figure 4c, and D is the magnetic declination. The relative magnitudes of sin$D$ and cos$D$ are given in Table 1.

Figure 5c shows geographic zonal winds calculated from the FLIP model equivalent winds using the assumption that there is no longitudinal variation in the geographic meridian wind. There is remarkably good

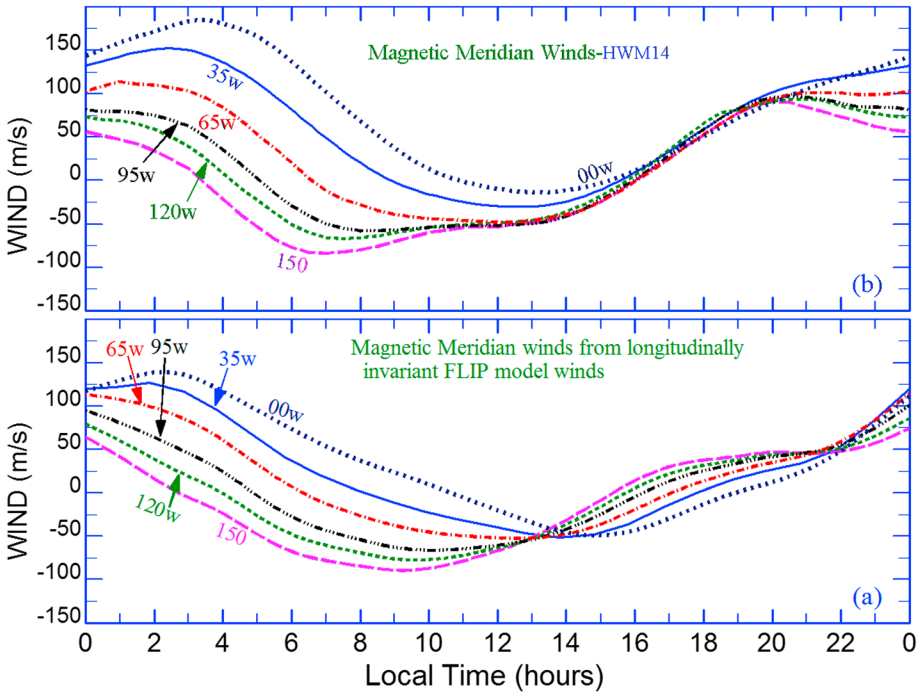

Figure 6. Magnetic meridian neutral winds at 65°S latitude and 0°W, 35°W, 64°W, 95°W, 120°W, and 150°W longitudes. (a) The magnetic meridian winds calculated from the 35°W equivalent wind and the median zonal wind from Figure 5c assuming no longitudinal variation. (b) The HWM14 magnetic meridian winds. All of the winds are determined from medians over 1–18 January 2007–2010.

agreement between the HWM14 zonal winds in Figure 5b and the zonal winds in Figure 5c. This is further demonstrated by the open circles in Figure 5b, which represent the median of the FLIP model zonal winds in Figure 5c. Some of the differences in the calculated zonal winds may result from the sensitivity to small errors in W_{eq} and W_{mer} when the sin$D$ is small. The sources of uncertainties in the equivalent winds are discussed in the FLIP model section (section 3).

4.4. Magnetic Declination, Inclination, and Neutral Winds

We next investigate the role of the magnetic field configuration in the longitudinal variation of h_mF_2 across the WSA. To isolate this effect, it is necessary to use geographic zonal and meridional winds that do not vary with longitude. For this purpose, we combine the FLIP model meridional wind at 35°W with a median FLIP model zonal wind (open circles) in Figure 5b. Once again, we primarily focus on the differences between noon and midnight.

Figure 6a shows the new magnetic meridian winds that were obtained by combining the 35°W meridional winds (circles in Figure 5a) with the median of the FLIP model geographic zonal winds (circles in Figure 5b). These winds compare well with the original FLIP model magnetic meridian winds shown in Figure 4c. Between noon and midnight there is very good agreement in the heart of the WSA, but the new magnetic meridional winds differ at the edges of the WSA due to the declination effect. The new FLIP model magnetic meridian winds have a striking resemblance to the HWM14 magnetic meridional winds that are displayed in Figure 6b. Given that this calculation assumed that there is no longitudinal variation in the geographic winds, it is clear that the magnetic declination effect is responsible for the midnight to noon phase shifts evident in Figures 4c, 6a, and 6b. The most important difference between the FLIP model and HWM14 winds is that HWM14 wind speeds are as much as 50 m s^{-1} greater than the FLIP model wind speeds in the crucial period between ~18 LT and midnight. This leads to much higher electron densities at midnight.

The inclination angle of the magnetic field can also contribute to the longitudinal variation of electron density across the WSA by changing the wind component parallel to the magnetic field by the factor

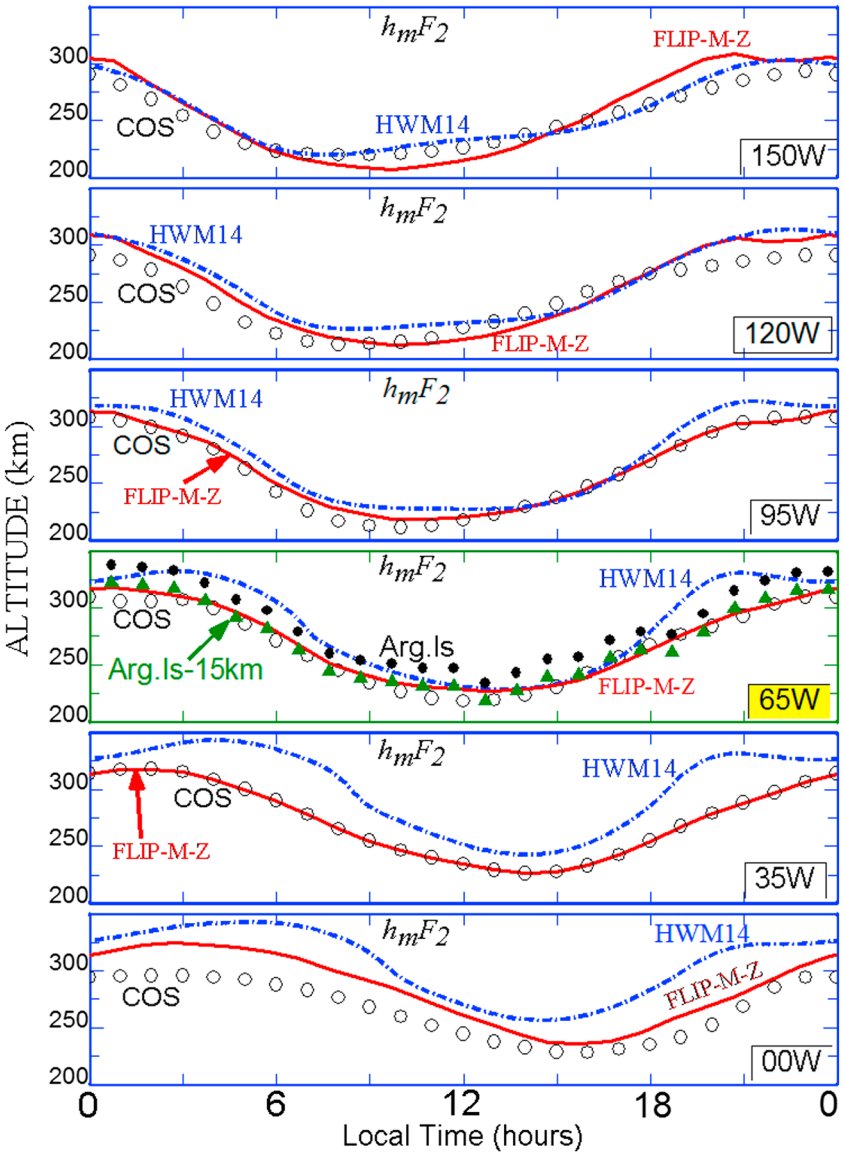

Figure 7. The calculated h_mF_2 when the FLIP model uses (1) HWM14 winds (dot-dash) and (2) the FLIP model winds from Figure 5a that assume that the 35°W wind is purely in the geographic meridian and there is no longitudinal variation in the geographic meridional and zonal winds (solid line). The open circles are the COSMIC h_mF_2 data for 1–18 January of 2007 to 2010 plotted on the hour. The full circles show the Argentine Islands solar minimum (1975–1977 and 1985–1987) median ionosonde data for 1–15 January. The green triangles show the Argentine Islands h_mF_2 data reduced by 15 km.

sin*I* cos*I*, where *I* is the magnetic inclination. The reduction of the electron density on the eastern side of the anomaly cannot be related to inclination because there is negligible change between 00°W and 95°W. However, on the western side of the WSA, the inclination increases from 63° at 95°W to 75° at 150°W. As a result, the effectiveness of the horizontal neutral wind in raising or lowering h_mF_2 will be reduced by a factor of 0.85 at 120°W and 0.61 at 150°W relative to 95°W (see Table 1).

4.5. Effect of Neutral Winds on h_mF_2

The magnetic meridional winds (assuming longitudinally invariant geographical wind components) of Figure 6a were used in the FLIP model to calculate the h_mF_2 that is shown by the solid red lines in Figure 7 at each longitude. The open circles show the COSMIC h_mF_2. The solid circles at 65°W show the median solar minimum h_mF_2 data from the Argentine Islands. The solid triangles show that there is very good agreement

with the Argentine Islands data when it is reduced by 15 km at all local times. Figure 7 also shows the FLIP model h_mF_2 calculations that were obtained when using the HWM14 (dash-dotted lines) wind model.

These longitudinally invariant FLIP model winds produce excellent agreement with the COSMIC data at 35°W, 65°W, and 95°W, but they overestimate h_mF_2 at 00°W, 120°W, and 150°W. Unless there is a systematic longitudinal error in the COSMIC h_mF_2 data, these results demonstrate that the actual meridional and zonal winds must vary with longitude, which contradicts the hypothesis that there is no wind variation across the WSA. The h_mF_2 differences at the edges of the WSA are generally less than 25 km, but they cause the FLIP model to greatly overestimate N_mF_2 in the evening. A systematic 25 km difference in h_mF_2 corresponds to about 50 m/s difference in magnetic meridional wind speed at night. Between noon and midnight, the declination effect opposes the inclination effect on the winds when the declination is eastward as it is between 35°W and 150°W. The fact that the model overestimates the evening h_mF_2 at 120°W and 150°W means that the declination effect is stronger than the inclination effect. Thus, we conclude that the magnetic configuration proposed by earlier researchers cannot explain the reduction in the anomaly between 95°W and 150°W.

The HWM14 produces good h_mF_2 agreement with the COSMIC data at 150°W but overestimates h_mF_2 around midnight at other longitudes. Appendix A discusses the reasons for the differences between the HWM models. The higher h_mF_2 from the Argentine Islands ionosonde may indicate that the nighttime neutral wind speeds are smaller than in previous solar minima during this period of unusually low solar activity. It may be thought that other possible combinations of longitudinally invariant geographic zonal and meridional winds could produce the observed longitudinal variation of h_mF_2. For example, the HWM14 model produces good results for h_mF_2 at 150°W. However, when those same geographic components are used as input for the FLIP model at all longitudes, they do not produce the observed variation of h_mF_2.

From this analysis, we conclude that longitudinal changes in the meridional and zonal wind speeds contribute to the enhanced nighttime h_mF_2 at in the heart of the WSA at 65°S latitude. An alternative perspective is that reduced winds cause a decrease in the electron density at the eastern and western edges of the WSA. The magnetic configuration does not explain why N_mF_2 decreases on the western edge of the WSA. While the inclination works to lower h_mF_2 on the western edge of the WSA, it is outweighed by the declination effect between noon and midnight.

4.6. The WSA N_mF_2 and Neutral Densities

Longitudinal variations in the neutral densities also play a role in the formation of the WSA. This is illustrated in Figure 8, which shows the COSMIC N_mF_2 data (open circles) and FLIP model calculations with longitudinally varying (green dashed lines) and when the 65°W neutral densities were used at all longitudes (dotted lines). Note that there is no dotted line on 65°W panel because it is the same as the green dashed line. The measured h_mF_2 was used as the wind proxy for all the N_mF_2 calculations in Figure 8. The model results are hourly medians that were obtained after running the model using the actual solar and magnetic activity for each year of the measurements. More details are provided in section 3.

There is very good agreement between the COSMIC satellite N_mF_2 data (open circles) and the solar minimum median ionosonde N_mF_2 data (solid circles) on the 65°W panel. The dash-dotted line at 65°W shows the model N_mF_2 that was calculated using the Argentine Islands solar minimum ionosonde h_mF_2 as the wind proxy. There is also excellent agreement between the data and the FLIP model for the Argentine Islands ionosonde N_mF_2.

When the neutral densities vary longitudinally as specified by NRLMSISE-00, there is very good agreement for 00°W and 35°W between noon and midnight, but the model increasingly underestimates the nighttime N_mF_2 with increasing westward longitude. Using the NRLMSISE-00 neutral densities for the fixed location of (65°S, 65°W) at every longitude (dotted lines) actually produced better agreement between the model and COSMIC N_mF_2 all the way from 35°W to 150°W, while the agreement was slightly degraded at 00°W.

Although the O to N_2 ratio would be expected to decrease with increasing proximity to the auroral energy input, the NRLMSISE-00 model appears to overestimate the longitudinal variation of the O to N_2 ratio as the magnetic latitude increases between 65°W and 150°W.

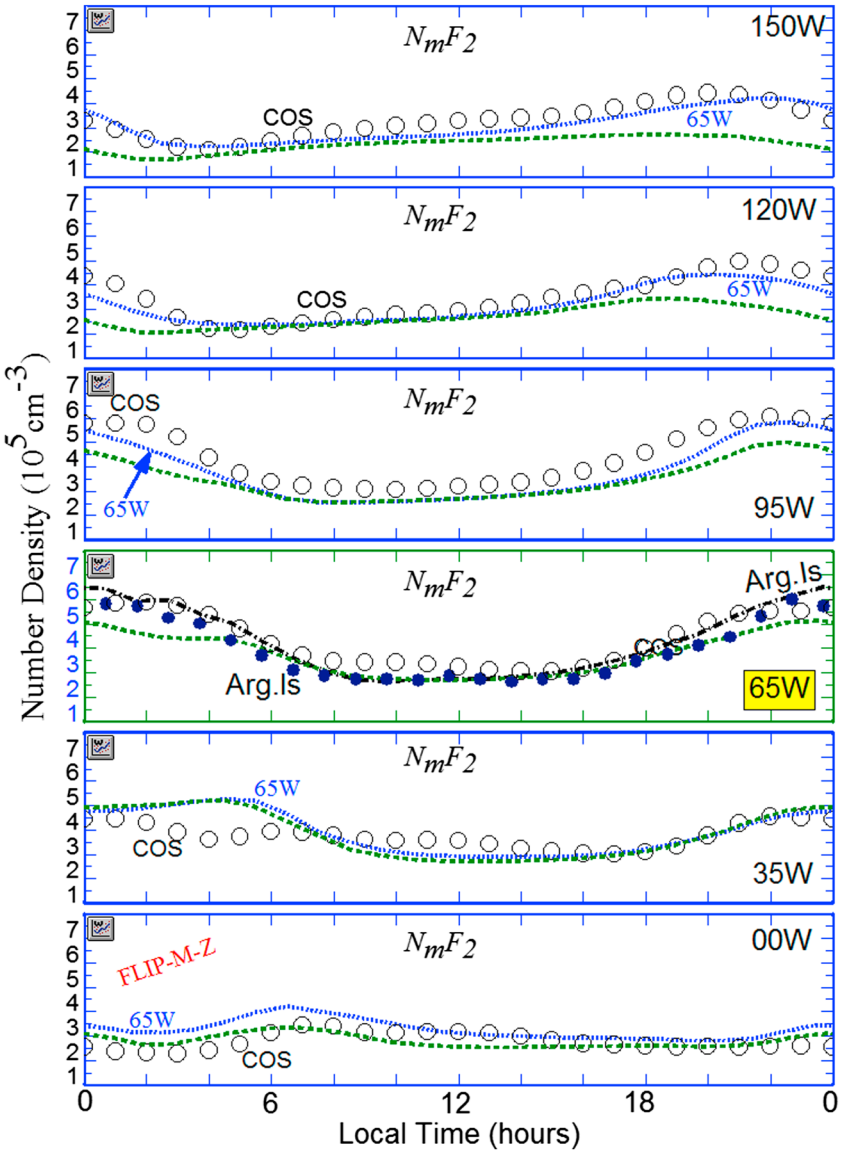

Figure 8. Effect of neutral densities on the model N_mF_2 at longitudes across the WSA using the COSMIC h_mF_2 as the wind proxy. The short dashed green line shows the calculations at all longitudes using the COSMIC h_mF_2 together with the actual NRLMSISE-00 model neutral densities at each longitude. The dotted lines labeled 65°W used the COSMIC h_mF_2 together with the NRLMSISE-00 model neutral densities for (65°S, 65°W) at all longitudes. The open circles are the COSMIC N_mF_2 data plotted on the hour. The solid circles on the 65°W panel show the solar minimum median N_mF_2 for the Argentine Islands and the black dash-dotted line shows the FLIP model calculation using the Argentine Islands median h_mF_2.

4.7. N_mF_2 and GUVI Neutral Densities and Temperatures

To further investigate the neutral density variations across the WSA, we compare GUVI satellite observations from 7 to 11 January 2007 with modeled neutral temperatures and density ratios. The solar and magnetic activity indices were low for this entire period. The lines in Figures 9 and 10 show the local time variations at different longitudes for the NRLMSIS00-E model of temperature (Figure 9b) and O/N_2 (Figure 10b). The corresponding TIMED-GUVI measurements near 14 LT are also shown.

The temperature and composition can be inferred from the FLIP model by running in the mode that determines what changes to the NRLMSISE-00 O to N_2 ratios are needed to reproduce the N_mF_2 data. The technique alters the O to N_2 ratio primarily by adjusting the exospheric temperature in the NRLMSISE-00 model. *Richards et al.* [2010] showed that the technique produces very good agreement with the GUVI data

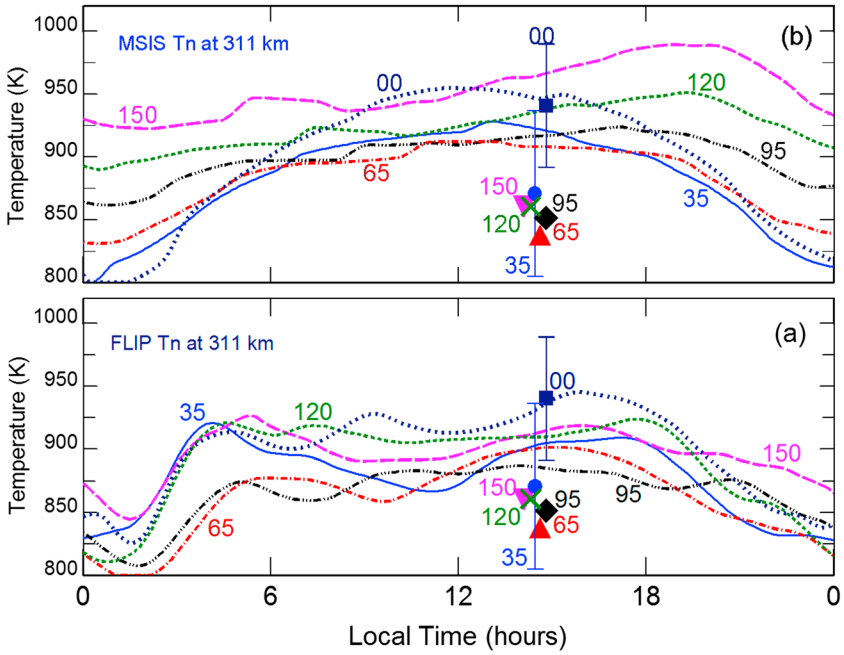

Figure 9. Model neutral temperatures at 311 km for the five longitudes. (b) The standard NRLMSISE-00 temperatures. (a) The temperatures were obtained by modifying the NRLMSISE-00 model to reproduce the COSMIC N_mF_2 and h_mF_2. The GUVI data symbols are color coded to match the lines 00°W (square with error bar), 35°W (dot with error bar), 64°W (triangle), 95°W (diamond), 120°W (cross), and 150°W (inverted triangle) longitudes. The GUVI values are averages for all the data, and the standard deviation error bars on the 00°W and 35°W data are representative of the data spread for all longitudes.

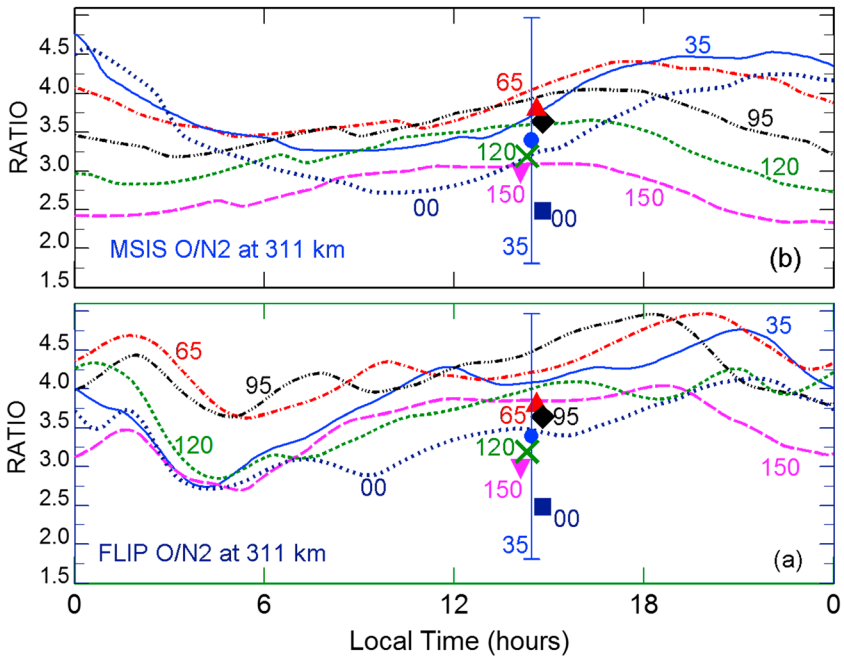

Figure 10. Model neutral O to N_2 ratios at 311 km for the five longitudes. (b) The standard NRLMSISE-00 neutral density ratios. (a) The ratios were obtained by modifying the MSIS model to reproduce the COSMIC N_mF_2 and h_mF_2. The GUVI data symbols are color coded to match the lines 00°W (square), 35°W (dot with error bar), 64°W (triangle), 95°W (diamond), 120°W (cross), and 150°W (inverted triangle) longitudes. The GUVI values are averages for all the data, and the standard deviation error bars on the 35°W data are representative of the data spread for all longitudes.

between 2000 and 2005, even during magnetic storms. The temperatures and O/N_2 ratios inferred by FLIP are shown in Figures 9a and 10a, respectively.

The COSMIC data are not ideal for comparison with the 2007 GUVI data because the former are averages over several years. In order to validate the FLIP model neutral density procedure for this period, the GUVI observations were compared with FLIP model calculations using ionosonde data from the Australian Ionospheric Prediction Service. There was very good agreement between the model and GUVI observations for both neutral temperatures and ratios for Canberra, Hobart, Norfolk Island, and Townsville. The model neutral density ratios are in particularly good agreement with the GUVI ratios for Christchurch (44°S, 173°E) which is closest to the WSA (see Appendix B).

The FLIP model was run for the entire 7–11 January 2007 period of the GUVI measurements using the COSMIC h_mF_2 as the wind proxy. For clarity of presentation, and because the COSMIC data are averages, the FLIP and NRLMSISE-00 model values are binned and shown for 10 January 2007. Similarly, the GUVI data are means for the entire period. The GUVI error bars are standard deviations from the means that reflect the scatter in the data. They are similar for all longitudes, but they are only plotted for 00°W and 35°W to avoid clutter. Figure 9a shows the diurnal variation of the FLIP modified neutral temperature, and Figure 9b shows the standard NRLMSISE-00 values for the six longitudes.

The temperatures and O to N_2 ratios at 00°W are clear outliers in the FLIP model and especially in the GUVI observations. Together with the lower h_mF_2 (wind speed) helps to explain the low COSMIC N_mF_2 at 00°W.

The GUVI and both model temperatures are lowest in the middle of the WSA and this leads to higher O to N_2 ratios (Figure 10), which increases the electron density. The two most notable aspects of the GUVI data are the small longitudinal variation in temperatures and that the density ratios are largest in the center of the WSA. The higher O to N_2 ratios in the center of the WSA are expected because of the greater displacement from the auroral energy input. At 14 LT, the percentage change in the NRLMSISE-00 temperatures with longitude is twice those of GUVI between 35°W and 150°W. On the other hand, the longitudinal variation in the FLIP modified temperature is comparable to that in the GUVI data near 14 LT. The GUVI data provide further support for the small longitudinal variations in density between 35°W and 150°W that are implied by Figure 8. There is very good agreement between the modified and standard temperatures and ratios in the evening at 00°W and 35°W.

The FLIP model modified temperatures and density ratios have much less variation with longitude than the NRLMSISE-00 model values. The modified temperatures also display less variation with local time. In particular, the FLIP modified temperatures are much lower between 18 LT and midnight. For similar geophysical conditions, higher temperatures usually correspond to smaller O to N_2 ratios at a given altitude because of the difference between the O and N_2 scale heights. Another key difference between the two model values is that the NRLMSISE-00 model has a distinct maximum temperature that migrates from midday at 35°W toward midnight at 150°W, while the FLIP model temperatures do not have a clearly defined phase shift. The longitudinal phase shift in NRLMSISE-00 disappears when the model parameters are plotted as a function of universal time, perhaps indicating that the longitudinal phase shift is related to displacement from the auroral energy input.

Figure 10 shows the longitudinal variation in the GUVI and FLIP O to N_2 ratios. The most important feature of the O to N_2 ratios is that they are highest in the center of the WSA and therefore are an important contributor to the high electron densities. The differences in the local time variations between the FLIP model estimates from the COSMIC observations and NRLMSIS00-E may suggest an additional semidiurnal or even terdiurnal variation during January at these latitudes that is not resolved in NRLMSIS00-E. Finally, it is important to note that the difference between the FLIP model ratios and the NRLMSIS00-E ratios is not large, being less than 25% during the day and increasing to ~40% before midnight at the boundaries of the WSA.

5. Summary and Conclusions

We have investigated physical mechanisms responsible for the longitudinal variation of the electron density across the Weddell Sea Anomaly where the *F* region midnight electron density exceeds the midday electron density. Specifically, we consider the region of the globe at 65°S latitude and between 00°W and

150°W longitude, which is outside of the auroral zone at magnetically quiet times. Of primary concern for the WSA is the local time between noon and midnight because the midnight N_mF_2 depends on the variation of the neutral wind and the neutral density during that time. The major difference from previous modeling studies is that observations are used to constrain certain key input parameters to the ionosphere model.

The overall conclusion is that the longitudinal variation of the nighttime N_mF_2 in the WSA is primarily caused by variations in both the neutral densities and the neutral winds via their changing proximity to the high-latitude energy input. There is little longitudinal variation in the midday N_mF_2. Contrary to previous suggestions, downward fluxes of ions from the plasmasphere do not contribute to the large densities in the WSA. In fact, the FLIP model shows that the topside H^+ actually flows upward at night, leading to a small net loss of O^+.

The contention that the magnetic field configuration is primarily responsible for the WSA is incomplete rather than wrong. It ignores likely changes in neutral densities and winds. Indeed, it is possible that the WSA exists only because it is in a magnetic midlatitude region that has extended sunlight hours. As a test of this hypothesis, we performed FLIP model simulations for several magnetic midlatitude stations (Christchurch, Hobart, Mundaring, Port Stanley, Wallops Island, Slough, Boulder, and Wakkanai) for summer conditions with the artificial restriction that the solar zenith angle does not exceed 93°. In all cases, the maximum N_mF_2 occurs near midnight and in several cases, it is nearly double the midday N_mF_2. Normally, the maximum N_mF_2 occurs near sunset at these stations and the midnight N_mF_2 is much lower than the midday N_mF_2 in summer. These simulations demonstrate that a particularly unusual magnetic inclination and declination are not required to explain the WSA.

The model and the data show that the longitudinal variation in the O to N_2 ratio maximizes in the center of the WSA, thus contributing to the higher electron density there. However, the NRLMSIS00-E model appears to overestimate the longitudinal temperature and density on the western edge of the WSA. The FLIP model-derived temperature and O/N_2 local time variations suggest higher-order local time variations that are not presently represented in NRLMSISE-00 climatology.

Significantly better agreement with the observed longitudinal N_mF_2 variation is obtained when the FLIP model instead keeps the neutral densities fixed at the 65°W values. Further support for the lower temperatures and densities results when the FLIP model is run in the mode that adjusts the model atmosphere to agree with the measured N_mF_2 as well as h_mF_2. Although the observed GUVI neutral density ratios and temperatures are variable, their median values also support smaller longitudinal variations than predicted by NRLMSIS00-E.

A notable neutral temperature and density ratio outlier occurs at 00°W longitude where both the model calculations and the GUVI data show that the temperature is ~75°K higher than at all other longitudes at 14 LT. The 00°W longitude is also a clear outlier with regard to h_mF_2 and with the equivalent neutral winds. The measured h_mF_2 at 00°W is ~25 km lower than at 35°W in the evening and the equivalent wind speed is ~50 m s^{-1} smaller as a result. The differences in density and wind behavior between 00°W and 150°W may reflect asymmetries in high-latitude energy input or in the way that energy is transferred from high to middle latitudes by general circulation patterns.

The role of the neutral winds is more complicated than neutral densities because changes can result from longitudinal changes in the meridional and zonal components as well as in the magnetic field declination and inclination. Our calculations indicate that longitudinal variation in one or both of the geographic wind components is most likely responsible for the longitudinal variation in h_mF_2 across the WSA. Changes in the magnetic field inclination are only important on the western edge of the WSA, but the inclination and declination effects on the wind components tend to oppose each other between noon and midnight. The declination influence on the wind does contribute to the decrease in h_mF_2 on the eastern edge. However, decreased wind speeds and O to N_2 ratios are more important for the decrease in electron density there.

There was remarkable similarity between the equivalent neutral winds determined from the measured h_mF_2 and the climatological HWM14 magnetic meridional neutral winds derived from other data sets. However, the HWM14 winds are as much as 50 m s^{-1} greater than the equivalent winds at night, which causes the

FLIP model to overestimate the nighttime h_mF_2 and therefore N_mF_2. Both the equivalent and HWM14 magnetic meridional winds show little longitudinal variation between noon and midnight, but there are substantial longitudinal differences between midnight and noon that result from the combined effects of different magnetic declination and large zonal wind speeds.

Since the equivalent winds may contain an electric drift component, it is possible that electric fields play a role in the longitudinal variations in the observed h_mF_2 and also explain some of the differences with the HWM models. However, this research does not support any requirement for horizontal transport of plasma by electric fields that were proposed by *Klimenko et al.* [2015]. This is because the high electron densities in the center of the WSA can be explained by in situ processes once the physical model reproduces the observed h_mF_2.

The HWM14 wind model produces good h_mF_2 agreement at some longitudes but there are significant differences at other longitudes. The lack of data to constrain the basis parameters of the empirical wind model in the main WSA region may be the reason. (See Appendix A.) One indirect implication of this study is that the equivalent winds from the FLIP modeling technique could provide important new wind information for future versions of the HWM model that reconcile this localized issue in HWM14, which would, in turn, enable improved understanding of the WSA.

In summary, we have (1) quantified the factors that lead to the WSA, (2) determined the longitudinal variation of the geographic zonal wind components using h_mF_2 data, (3) used h_mF_2 data as a constraint so that its effect on N_mF_2 can be determined, and (4) evaluated changes in neutral density in the WSA. This analysis leads to the conclusion that longitudinal changes in the neutral winds and neutral densities are important for the longitudinal variation in the WSA.

Appendix A: HWM Empirical Model Winds

Except at 150°W, the HWM14 model does not reproduce the observed longitudinal variation of the nighttime h_mF_2 for the localized region and time period considered in this study. Overall, HWM14 represents a major improvement over HWM07 globally [cf. *Drob et al.*, 2015, Table 1]. It is important to keep in mind that the model parameters of all HWM versions are estimated globally by a fitting a truncated set of Fourier-modulated vector spherical harmonics to all of the available satellite and ground-based data sets simultaneously, including all local times, day-of-year, latitudes, longitudes, altitudes, and solar cycle conditions. Figure A1 shows the data available in the vicinity of the WSA for January along with the nominal quiet time meridional winds on 15 January predicted by HWM93 (blue line), HWM07 (green line), and HWM14 (red line) at 275 km altitude at 65°S, 65°W. The dashed lines indicate projections of the HWM wind components into the direction of the magnetic meridian assuming a declination of 15°.

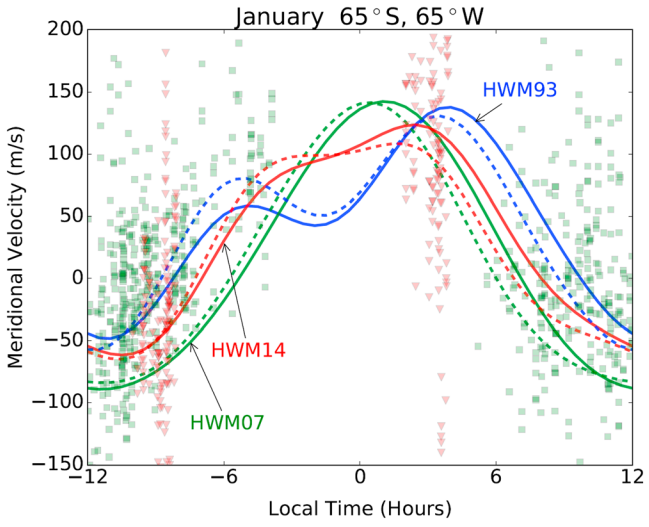

Figure A1. Comparison of the quiet time 15 January meridional winds at 275 km, 65°S, and 65°W from HWM93 (blue), HWM07 (green), and HWM14 (red), with the available historical WINDII 557.7 (green squares) and DE 2 FPI (red triangles) meridional wind measurements. The dashed lines represent the HWM winds projected into the magnetic meridian with a declination of 12°. Error bars for the observations ranging from ~30 to 75 m/s have been omitted for clarity. Only ~50% of the available WINDII 557.7 nm wind measurements for all January months from 1991 to 1996, between 245 and 350 km altitude, 65 ± 5°S latitude, and 65 ± 30°W longitude are shown. The available DE 2 FPI meridional wind measurements in January (1982 and 1983) between altitudes from 245 to 350 km and latitudes of 65 ± 7.5°S are shown.

The only available observations come from the Upper Atmospheric Research Satellite Wind Imaging Interferometer (WINDII) [*Shepherd*

et al., 1993] and the Dynamics Explorer 2, Fabry-Perot Interferometer (DE 2 FPI) [*Hays et al*., 1981]. WINDII measured both components of the daytime thermospheric vector wind between ±72° latitude from 1991 to 1996 using the thermospheric atomic oxygen 557.7 nm dayglow emission. Figure A1 shows approximately 50% of the available WINDII 557.7 nm meridional wind measurements (green squares) for altitudes between 245 and 350 km for the region between 65 ± 5°S latitude and 65 ± 30°W longitude. The DE 2 FPI measured the thermospheric meridional wind component from 1982 to 1983 from the atomic oxygen 630.0 nm dayglow and nightglow emissions. Figure A1 shows all of the January DE 2 FPI measurements (red triangles) between 245 and 350 km altitude and 65 ± 7.5°S (latitude). For both instruments the measurement uncertainties range from approximately 30 to 75 m/s. Here any observations with uncertainties greater than 100 m/s, when 3 h $A_p > 20$, or when $F_{10.7} \geq 150$ were excluded. When the HWM93 model was developed, only the DE 2 FPI and DE 2 Wind and Temperature Spectrometer zonal component wind observations [*Spencer et al*., 1981] (not shown here) were available for this location and time.

Note the lack of observations between approximately 20:00 and 01:00 locale time. Outside these hours the measurements also exhibit a high degree of variability. Thus, the climatological HWM parameter estimates are somewhat poorly constrained in the WSA region. Consequently, spurious behavior around local midnight can be produced by the model from the fitting of the observations in other regions of space and time period. More specifically, the differences between the HWM models and this local subset of data highlight are the result of necessary trade-offs between the model resolution that is required to avoid "overfitting" the data in data-poor regions and "underfitting" observations in other regions while attempting to match all the observations at adjacent altitudes, latitudes, and months. Thus, we suggest that the local time behavior in HWM14 (and HWM93) between 20:00 and 01:00 could be the consequence of spectral artifacts from over fitting of spectral components. Indeed, a preliminary analysis suggests that this artifact resides primarily in the HWM14 terdiunal tidal component at this latitude and season.

Lastly, Figure A1 also implies that the equivalent winds from the FLIP modeling technique could provide important new wind information for future versions of the HWM model to reconcile this localized issue in HWM14, which would, in turn, enable improved understanding of the WSA.

Appendix B: Validation of FLIP Model Neutral Composition Using Christchurch Data

The Argentine Islands would be the ideal location for investigation of neutral composition on N_mF_2 and h_mF_2 with coincident ionosonde, COSMIC, and GUVI observations, but the facility closed in 1996. Instead, we use 2007 ionosonde data from Australia and New Zealand for validation of the procedures. These ionosonde data have been carefully hand scaled for optimal accuracy. While these sites are outside the defined WSA, the comparison supports the neutral composition analysis.

Figure B1 shows a comparison of the modeled and measured N_mF_2, h_mF_2, O to N_2 ratio, and neutral temperature at Christchurch, New Zealand (44°S, 173°E), for 8–11 January 2007. The closed red circles without error bars show the ionosonde data for 8–11 January 2007. There is very good agreement between the median 2007–2010 COSMIC N_mF_2 (open circles) and the median ionosonde N_mF_2 for 1–18 January 2007–2010 (asterisks). However, the median COSMIC h_mF_2 is 10–15 km lower than the median ionosonde h_mF_2.

The solid blue lines in Figure B1 are from a FLIP model simulation that uses the standard NRLMSISE-00 model and the ionosonde h_mF_2 as the wind proxy. The FLIP model N_mF_2 underestimates the 2007 ionosonde data just before noon, but there is good agreement at the time of the GUVI measurements. A point worth noting is that the measured and modeled N_mF_2 increases throughout the day until it maximizes near local sunset. That suggests that N_mF_2 would peak near midnight if the solar zenith angle variation were similar to that at the Argentine Islands. This further emphasizes the need to bin N_mF_2 data closer to midnight and midday when studying the Weddell Sea Anomaly.

Figures B1c and B1d show the model and the GUVI (symbols with error bars) neutral temperature and O to N_2 density ratio at 311 km altitude. The solid blue lines are from the standard NRLMSISE-00 model, while the dashed red lines are values obtained by the FLIP model when the neutral densities are modified so that the model follows the observed N_mF_2, as well as h_mF_2. Coincidentally, the GUVI

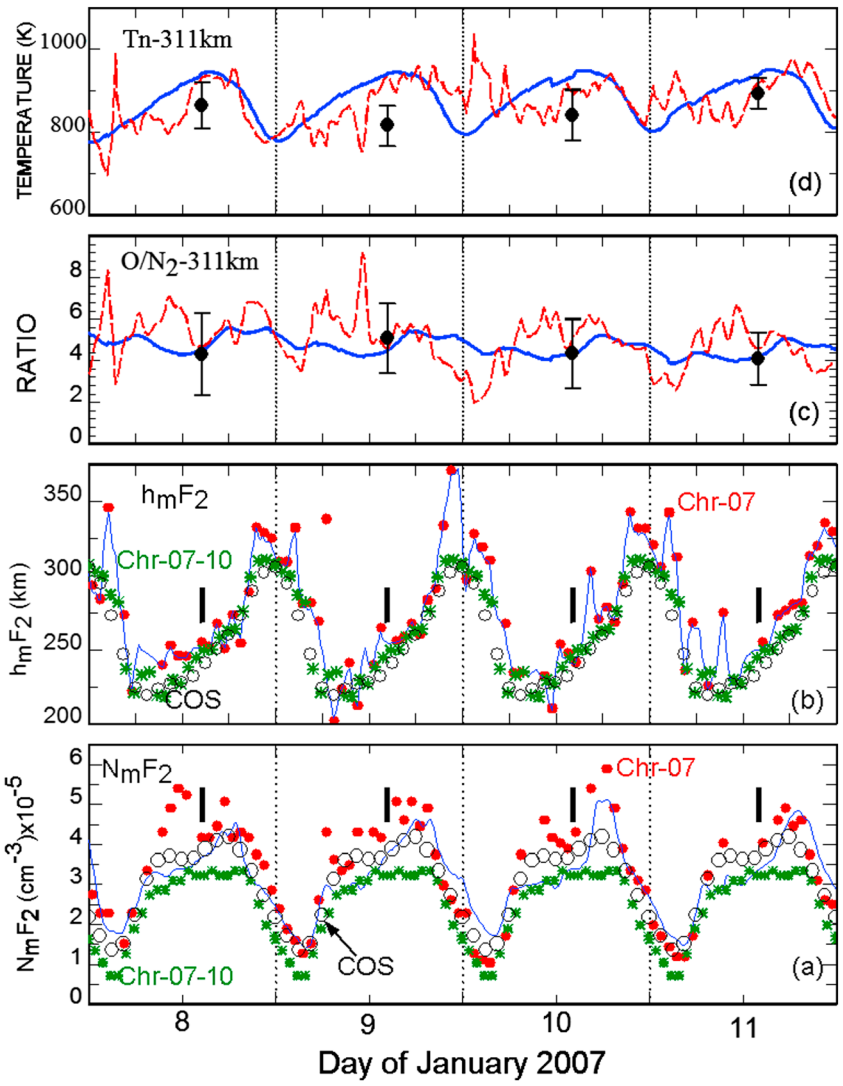

Figure B1. Comparison of modeled and measured (a) N_mF_2, (b) h_mF_2, (c) O to N_2 ratio, and (d) neutral temperature at Christchurch (44°S, 173°E) for 8–11 January 2007. The closed red circles show the ionosonde data for 8–11 January 2007. The solid blue lines are from the FLIP model using the standard NRLMSISE-00 model and the 2007 ionosonde h_mF_2 as the wind proxy. The open circles show the 2007–2010 COSMIC data, and the asterisks show the 2007–2010 median ionosonde data. The dashed red lines in Figures B1c and B1d are from the FLIP model neutral density modification algorithm. The symbols with error bars show the TIMED-GUVI neutral temperature and O to N_2 density ratios. The black vertical marks in Figures B1a and B1b indicate the times of the GUVI data. The vertical grid lines are at midnight LT.

observations occur when the FLIP model is in best agreement with the ionosonde observations so the modification to the neutral densities is smallest. There is excellent agreement between the GUVI and model O/N_2 ratio, but the GUVI temperature is ~50°K lower than the FLIP model temperature on the first 3 days, although still within the statistical error. It must be noted that the FLIP model derived O/N_2 ratio is more accurate than the derived neutral temperature because the O/N_2 ratio primarily determines N_mF_2.

Additional model calculations were made for six Australian ionosonde stations that are widely spaced in latitude and longitude. The model agreement with the GUVI Tn and O/N_2 data is comparable to that for Christchurch at all six stations. In particular, there is little difference in h_mF_2 and N_mF_2 between the Christchurch (44°S, 173°E) and Hobart (43°S, 147°E) ionosonde data.

These comparisons provide confidence in the procedures when applied to the WSA region.

Acknowledgments

P.G.R. and R.R.M. were supported by NASA grant NNX15AI90G to George Mason University. D.P.D. was supported by the Chief of Naval Research, through the NRL 6.1 basic research program. The complete 1961 to 1990 ionosonde database is available on a CD-ROM from http://www.ngdc.noaa.gov/stp/cdrom/ionocd.html. Ionosonde data up to the present are available from the National Geophysical Data Center at http://spidr.ngdc.noaa.gov/spidr/. This study also uses ionosonde data from the Australian Bureau of Meteorology Space Weather Network (http://www.sws.bom.gov.au/). Software developed by the authors to extract the CD-ROM data and the FLIP model are available from the authors upon request. The Atmosphere Explorer satellite data are available from http://omniweb.gsfc.nasa.gov/ftpbrowser/atmoweb.html. The complete unified abstracts data set and software to conveniently access the data are available from the authors. Version 10 GUVI limb data products were produced by R. R. Meier and are available via the GUVI website (guvi.jhuapl.edu and http://vitmo.jhuapl.edu/index.php?action=sitePages/about.php). GUVI O/N_2 column density ratios on the disk are available through the present. The raw observations are processed in both near real time and postprocess mode and stored at the COSMIC Data Analysis and Archive Center (CDAAC). The solar EUV irradiances irradiance measurements that were obtained from the LASP Interactive Solar Irradiance Data Center (LISIRD). The International Geomagnetic Reference Field (IGRF) model parameters are at http://omniweb.gsfc.nasa.gov/vitmo/cgm_vitmo.html.

References

Anderson, C., M. J. Kosch, M. J. Nicolls, and M. Conde (2012), Ion-neutral coupling in Earth's thermosphere, estimated from concurrent radar and optical observations above Alaska, *J. Atmos. Sol. Terr. Phys.*, *105–106*, 313–324, doi:10.1016/j.jastp.2013.04.005.

Bellchambers, W. H., and W. R. Piggott (1958), Ionospheric measurements made at Halley Bay, *Nature*, *182*, 1596–1597, doi:10.1038/1821596a0.

Bilitza, D. (2015), The International Reference Ionosphere—Status 2013, *Adv. Space Res.*, *55*, 1914–1927.

Bilitza, D., R. Eyfrig, and N. M. Sheikh (1979), A global model for the height of the F_2-peak using *M*3000 values from the CCIR numerical map, *Telecommun. J.*, *46*, 549–553.

Burns, A. G., Z. Zeng, W. Wang, J. Lei, S. C. Solomon, A. D. Richmond, T. L. Killen, and Y.-H. Kuo (2008), Behavior of the F_2 peak ionosphere over the South Pacific at dusk during quiet summer condition from COSMIC data, *J. Geophys. Res.*, *113*, A12305, doi:10.1029/2008JA013308.

Burns, A. G., S. C. Solomon, W. Wang, G. Jee, C. H. Lin, C. Rocken, and Y. H. Kuo (2011), The summer evening anomaly and conjugate effects, *J. Geophys. Res.*, *116*, A01311, doi:10.1029/2010JA015648.

Burnside, R. G., C. A. Tepley, and V. B. Wickwar (1987), The O^+-O collision cross-section: Can it be inferred from aeronomical measurements?, *Ann. Geophys., Ser. A*, *5*(6), 343.

Chang, L. C., H. Liu, Y. Miyoshi, C.-H. Chen, F.-Y. Chang, C.-H. Lin, J.-Y. Liu, and Y.-Y. Sun (2015), Structure and origins of the Weddell Sea Anomaly from tidal and planetary wave signatures in FORMOSAT-3/COSMIC observations and GAIA GCM simulations, *J. Geophys. Res. Space Physics*, *120*, 1325–1340, doi:10.1002/2014JA020752.

Chapman, S. (1931), The absorption and dissociative or ionizing effect of monochromatic radiation in an atmosphere on a rotating earth, *Proc. Phys. Soc.*, *43*(1), 26.

Chen, C. H., J. D. Huba, A. Saito, C. H. Lin, and J. Y. Liu (2011), Theoretical study of the ionospheric Weddell Sea Anomaly using SAMI2, *J. Geophys. Res.*, *116*, A04305, doi:10.1029/2010JA015573.

Chen, Y., L. Liu, H. Le, W. Wan, and H. Zhang (2016), The global distribution of the dusk-to-nighttime enhancement of summer N_mF_2 at solar minimum, *J. Geophys. Res. Space Physics*, *121*, 7914–7922, doi:10.1002/2016JA022670.

Christensen, A. B., et al. (2003), Initial observations with the global Ultraviolet Imager (GUVI) in the NASA TIMED satellite mission, *J. Geophys. Res.*, *108*(A12), 1451, doi:10.1029/2003JA009918.

Drob, D. P., et al. (2015), An update to the horizontal wind model (HWM): The quiet time thermosphere, *Earth Space Sci.*, *2*, 301–319, doi:10.1002/2014EA000089.

Dudeney, J. R. (1983), The accuracy of simple methods for determining the height of the maximum electron concentration of the F_2-layer from scaled ionospheric characteristics, *J. Atmos. Terr. Phys.*, *45*, 629.

Dyson, P. L., T. P. Davies, M. L. Parkinson, A. J. Reeves, P. G. Richards, and C. E. Fairchild (1997), Thermospheric neutral winds at southern mid-latitudes: A comparison of optical and ionosonde h_mF_2 methods, *J. Geophys. Res.*, *102*, 27,189.

Emmert, J. T., R. R. Meier, J. M. Picone, J. L. Lean, and A. B. Christensen (2006), Thermospheric density 2002–2004: TIMED/GUVI dayside limb observations and satellite drag, *J. Geophys. Res.*, *111*, A10S16, doi:10.1029/2005JA011495.

Emmert, J. T., S. E. McDonald, D. P. Drob, R. R. Meier, J. L. Lean, and J. M. Picone (2014), Attribution of interminima changes in the global thermosphere and ionosphere, *J. Geophys. Res. Space Physics*, *119*, 6657–6688, doi:10.1002/2013JA019484.

Fuller-Rowell, T. J., D. Rees, S. Quegan, R. J. Moffett, M. V. Codrescu, and G. H. Millward (1996), A coupled thermosphere-ionosphere model (CTIM), in *STEP Handbook of Ionospheric Models*, edited by R. W. Schunk, pp. 217–238, Utah State Univ. Press, Logan.

Hays, P. B., T. L. Killeen, and B. C. Kennedy (1981), The Fabry-Perot Interferometer on Dynamics Explorer, *Space Sci. Instrum.*, *5*, 395–416.

He, M., L. Liu, W. Wan, B. Ning, B. Zhao, J. Wen, X. Yue, and H. Le (2009), A study of the Weddell Sea Anomaly observed by FORMOSAT-3/COSMIC, *J. Geophys. Res.*, *114*, A12309, doi:10.1029/2009JA014175.

Horvath, I. (2006), A total electron content space weather study of the nighttime Weddell Sea Anomaly of 1996/1997 southern summer with TOPEX/Poseidon radar altimetry, *J. Geophys. Res.*, *111*, A12317, doi:10.1029/2006JA011679.

Horvath, I., and E. A. Essex (2003), The Weddell Sea Anomaly observed with the TOPEX satellite data, *J. Atmos. Sol. Terr. Phys.*, *65*(6), 693–706, doi:10.1016/S1364-6826(03)00083-X.

Hsu, M. L., C. H. Lin, R. R. Hsu, J. Y. Liu, L. J. Paxton, H. T. Su, H. F. Tsai, P. K. Rajesh, and C. H. Chen (2011), The OI 135.6 nm airglow observations of the midlatitude summer nighttime anomaly by TIMED/GUVI, *J. Geophys. Res.*, *116*, A07313, doi:10.1029/2010JA016150.

Huba, J. D., G. Joyce, and J. A. Fedder (2000), SAMI2 is another model of the ionosphere (SAMI2): A new low-latitude ionosphere model, *J. Geophys. Res.*, *105*, 23,035–23,054, doi:10.1029/2000JA000035.

Jee, G., W. W. Schunk, and L. Scherliess (2005), On the sensitivity of total electron content (TEC) to upper atmospheric/ionospheric parameters, *J. Atmos. Terr. Phys.*, *67*, 1040–1052.

Jee, G., A. G. Burns, Y.-H. Kim, and W. Wang (2009), Seasonal and solar activity variations of the Weddell Sea Anomaly observed in the TOPEX total electron content measurements, *J. Geophys. Res.*, *114*, A04307, doi:10.1029/2008JA013801.

Karpachev, A. T., N. A. Gasilov, and O. A. Karpachev (2010), Causes of N_mF_2 longitudinal variations at mid and subauroral latitudes under summer nighttime conditions, *Geomagn. Aeron.*, *50*(4), 482–488, doi:10.1134/S0016793210040092.

Karpachev, N., A. Gasilov, and O. A. Karpachev (2011), Morphology and causes of the Weddell Sea Anomaly 2011, *Geomagn. Aeron.*, *51*(6), 812–824, doi:10.1134/S0016793211050070.

Klimenko, M. V., V. V. Klimenko, and A. T. Karpachev (2015), Spatial features of Weddell Sea and Yakutsk Anomalies in f_oF_2 diurnal variations during high solar activity periods: Interkosmos-19 satellite and ground-based ionosonde observations, IRI reproduction and GSM TIP model simulation, *Adv. Space Res.*, *55*, 2020–2032, doi:10.1016/j.asr.2014.12.032.

Kotov, D. V., V. Truhlík, P. G. Richards, S. Stankov, O. V. Bogomaz, L. F. Chernogor, and I. F. Domnin (2015), Night-time light ion transition height behaviour over the Kharkiv (50°N, 36°E) IS radar during the equinoxes of 2006–2010, *J. Atmos. Sol. Terr. Phys.*, *132*, 1–12, doi:10.1016/j.jastp.2015.06.004.

Lin, C. H., J. Y. Liu, C. Z. Cheng, C. H. Chen, C. H. Liu, W. Wang, A. G. Burns, and J. Lei (2009), Three-dimensional ionospheric electron density structure of the Weddell Sea Anomaly, *J. Geophys. Res.*, *114*, A02312, doi:10.1029/2008JA013455.

Lin, C. H., C. H. Liu, J. Y. Liu, C. H. Chen, A. G. Burns, and W. Wang (2010), Midlatitude summer nighttime anomaly of the ionospheric electron density observed by FORMOSAT-3/COSMIC, *J. Geophys. Res.*, *115*, A03308, doi:10.1029/2009JA014084.

Liu, L., H. Le, Y. Chen, M. He, W. Wan, and X. Yue (2011), Features of the middle- and low-latitude ionosphere during solar minimum as revealed from COSMIC radio occultation measurements, *J. Geophys. Res.*, *116*, A09307, doi:10.1029/2011JA016691.

Meier, R. R., et al. (2015), Remote sensing of Earth's limb by TIMED/GUVI: Retrieval of thermospheric composition and temperature, *Earth Space Sci.*, *2*, 1–37, doi:10.1002/2014EA000035.

Nicolls, M. J., N. Aponte, S. A. Gonzalez, M. P. Sulzer, and W. L. Oliver (2006), Daytime *F* region ion energy balance at Arecibo for moderate to high solar flux conditions, *J. Geophys. Res.*, *111*, A10307, doi:10.1029/2006JA011664.

Picone, J. M., A. E. Hedin, D. P. Drob, and A. C. Aikin (2002), NRLMSISE-00 empirical model of the atmosphere: Statistical comparisons and scientific issues, *J. Geophys. Res.*, *107*(A12), 1468, doi:10.1029/2002JA009430.

Ren, Z., W. Wan, L. Liu, H. Le, and M. He (2012), Simulated midlatitude summer nighttime anomaly in realistic geomagnetic fields, *J. Geophys. Res.*, *117*, A03323, doi:10.1029/2011JA017010.

Richards, P. G. (1991), An improved algorithm for determining neutral winds from the height of the F_2 peak electron density, *J. Geophys. Res.*, *96*, 17,839.

Richards, P. G. (2001), Seasonal and solar cycle variations of the ionospheric peak electron density: Comparison of measurement and models, *J. Geophys. Res.*, *106*, 12,803.

Richards, P. G. (2002), Ion and neutral density variations during ionospheric storms in September 1974: Comparison of measurement and models, *J. Geophys. Res.*, *107*(A11), 1361, doi:10.1029/2002JA009278.

Richards, P. G. (2004), On the increases in nitric oxide density at mid latitudes during ionospheric storms, *J. Geophys. Res.*, *109*, A06304, doi:10.1029/2003JA010110.

Richards, P. G., and P. J. Wilkinson (1998), The ionosphere and thermosphere at southern mid-latitudes during the November l993 ionospheric storm: A comparison of measurement and modeling, *J. Geophys. Res.*, *103*, 9373.

Richards, P. G., P. L. Dyson, T. P. Davies, M. L. Parkinson, and A. J. Reeves (1998), The behavior of the ionosphere and thermosphere at a southern mid-latitude station during magnetic storms in early March 1995, *J. Geophys. Res.*, *103*, 26,421.

Richards, P. G., et al. (2000), On the relative importance of convection and temperature on the behavior of the ionosphere in North America during January, 6–12, l997, *J. Geophys. Res.*, *105*, 12,763–12,776.

Richards, P. G., M. J. Nicolls, C. J. Heinselman, J. J. Sojka, J. M. Holt, and R. R. Meier (2009), Measured and modeled ionospheric densities, temperatures, and winds during the IPY, *J. Geophys. Res.*, *114*, A12317, doi:10.1029/2009JA014625.

Richards, P. G., R. R. Meier, and P. J. Wilkinson (2010), On the consistency of satellite measurements of thermospheric composition and solar EUV irradiance with Australian ionosonde electron density data, *J. Geophys. Res.*, *115*, A10309, doi:10.1029/2010JA015368.

Richards, P. G., M. J. Nicolls, J.-P. St.-Maurice, L. Goodwin, and J. M. Ruohoniemi (2014), Investigation of sudden electron density depletions observed in the dusk sector by the Poker Flat, Alaska incoherent scatter radar in summer, *J. Geophys. Res. Space Physics*, *119*, 10,608–10,620, doi:10.1002/2014JA020541.

Rishbeth, H., and O. K. Garriott (1969), *Introduction to Ionospheric Physics*, 60 pp., Academic Press, San Diego, Calif.

Rishbeth, H. (1972), Thermospheric winds and the *F*-region: A review, *J. Atmos. Terr. Phys.*, *34*, 1.

Salah, J. E. (1993), Interim standard for the ion-neutral atomic oxygen collision frequency, *Geophys. Res. Lett.*, *20*, 1543.

Schunk, R. W., and J. C. G. Walker (1973), Theoretical ion densities in the lower ionosphere, *Planet. Space Sci.*, *21*, 1875–1896.

Shepherd, G. G., et al. (1993), WINDII, the Wind Imaging Interferometer for the Upper Atmosphere Research Satellite, *J. Geophys. Res.*, *98*, 10,725–10,750.

Spencer, N. W. L. E., H. B. Wharton, A. E. Niemann, G. R. C. Hedin, and J. C. Maurer (1981), The Dynamics Explorer wind and temperature spectometer, *Space Sci. Instrum.*, *5*, 417–428.

Torr, M. R., D. G. Torr, P. G. Richards, and S. P. Yung (1990), Mid- and low-latitude model of thermospheric emissions, 1, O+(2P) 7320 Å and N_2 (2P) 3371 Å, *J. Geophys. Res.*, *95*, 21,147.

Woods, T. N., et al. (2008), XUV photometer system (XPS): Improved solar irradiance algorithm using Chianti spectral models, *Sol. Phys.*, *250*, 235–267, doi:10.1007/s11207-008-9196-6.

Wu, Q., W. Wang, R. G. Roble, I. Häggström, and A. Strømme (2012), First daytime thermospheric wind observation from a balloon-borne Fabry–Perot Interferometer over Kiruna (68°N), *Geophys. Res. Lett.*, *39*, L14104, doi:10.1029/2012GL052533.

Yue, X., W. S. Schreiner, J. Lei, C. Rocken, D. C. Hunt, Y.-H. Kuo, and W. Wan (2010), Global ionospheric response observed by COSMIC satellites during the January 2009 stratospheric sudden warming event, *J. Geophys. Res.*, *115*, A00G09, doi:10.1029/2010JA015466.